BIOMECHANICAL DEFORMABLE REGISTRATION FOR DEEP BRAIN STIMULATION

Fotis Drakopoulos[1], Michael Weissberger[2], Kathryn Holloway[3], and Nikos Chrisochoides[1]

[1]CRTC Lab and Computer Science, Old Dominion University, Norfolk, VA
[2]VCU School of Medicine, Richmond, VA
[3]Neurosurgical Section of SE PADRECC McGuire VAMC, Richmond, VA

Keywords: Deformable Registration, Medical Imaging, Deep Brain Stimulation, Stereotactic surgery

Abstract

In this paper we present an adaptive deformable registration method for Deep Brain Stimulation. The method relies on hexahedral mesh generation to compensate for the noise of CT scans. An adaptive approach is utilized to improve the accuracy of a well known non-rigid registration method used extensively for registration of MRI data. Finally parallel computing is used to reduce the execution time introduced due to adaptivity. Our evaluation on three DBS cases indicates that the proposed scheme satisfies the real-time constraints of DBS surgery and recovers the deep-brain deformation with high fidelity. Understanding brain shift in this context is an important task to improve the patient outcomes in DBS surgery.

1. INTRODUCTION

Deep brain stimulation (DBS) is an effective palliative therapy for patients suffering from Essential Tremor, Parkinson's disease, and other neurological movement disorders. As an adjunct to medical intervention, DBS therapy can reduce the morbidity associated with these disorders significantly [11]. DBS surgery involves the placement of electrical leads into precise locations in the deep structures of the brain, without direct intra-operative visualization of the target structures or of the electrode lead. Modern DBS surgery makes use of stereotactic systems and image guidance to accurately place electrode leads, as well as intra-operative imaging to surveil the location of the lead and guide the surgery. The effectiveness of DBS is directly correlated with the accuracy of DBS electrode lead placement, with more accurate electrode placement leading to better clinical outcomes. Rarely, re-operation is necessary to correct the placement of a DBS lead (1% to 12.7%)[1, 4, 9, 8]. The targets of the DBS surgery are located in the basal ganglia, a structure that helps regulate movement and is central to the pathology of Parkinson's disease. The basal ganglia itself includes the subthalamic nucleus (STN) and globus pallidus internus (GPi), two of the targets of DBS surgery [12, 13].

Compounding the relatively small size and deep location of these nuclei is the fact that they are often moving targets during surgery. The phenomenon of brain shift is well documented during DBS and other procedures that result in CSF leakage. Previous studies have shown a brain shift during DBS surgery of up to 4mm in deep brain structures, 13mm in cortical structures, and development of a pneumocephalus in early post-surgery of up to 20mm. In addition to intra-operative shift, there is evidence that as subdural air collections resolve in the weeks after surgery, these leads may continue to shift [12, 13]. This shift complicates the placement of the DBS electrode leads, because the target nuclei are not visible on intra-operative CT, the modality commonly available in community and academic medical centers. The accurate modeling and correction for intra-operative brain shift during DBS surgery is essential for the improvement of surgical outcomes.

In this paper we propose a method to detect and quantify brain shift during DBS surgery using pre-operative (CT, MRI) and intra-operative (O-arm CT) imaging as inputs to a patient-specific biomechanical adaptive deformable (or non-rigid) registration algorithm [7]. In essence, this approach compares pre-operative and intra-operative images, detecting their movement, and inferring the unknown position of the surgical targets after brain shift using the deformation recovered from these landmarks.

In this work we describe a method to detect the brain shift that occurs during DBS surgery both qualitatively and quantitatively. The average brain shift of 2mm in the area of interest is at the boundary of resolution for this biomechanical deformable registration method, however, the presence of a highly radiolucent flexible intracranial fiducial (the stimulating electrode) improves the accuracy of this method. This effect is greatest precisely where it is most needed; near the deep-brain targets of DBS surgery. We use this fiducial as a gross landmark in the registration process that allows us to recover the detailed deformation of the electrode and the surrounding solid tissues. Finally, we employ recent advancements in computational power and the availability of powerful multi-processing GPU hardware to make the intra-operative use of these algorithms feasible and cost-effective. This high-performance computing architecture is widely available and a good candidate for intra-operative use.

2. PATIENTS AND METHODS

Three patients were included in this study. All patients had Parkinson's disease that was refractory to medical management and were treated with DBS surgery. All patients were treated at VCUHS Medical Center hospital or the VA McGuire Medical Center in Richmond. Patients were selected for this retrospective study based on several criteria: (i) amount of intracranial postoperative air, (ii) presence of bilateral air, (iii) amount of brain shift, and (iv) availability of pre-operative images (MRI, CT), intra-operative images (O-arm CT) at appropriate procedural intervals, and post-operative images (CT). The image size and spacing of the acquired clinical O-arm CT data is: $512 \times 512 \times 192$ (voxels^3), and $0.415 \times 0.415 \times 0.833$ (mm^3), respectively.

2.1. Procedural Methods

Pre-operative images for all patients were obtained, including fine-cut cone-beam CT, volumetric T1, T2, and FLAIR MRI protocols. Additionally, the placement of six bony fiducials in the patient's scalp assists in later rigid registrations. A stereotactic plan was created using these images. The NexFrame stereotactic system by Medtronic, Inc. was used for all cases. Next, the stereotactic space was registered to the image space using the previously placed bony fiducials while optimizing registration accuracy. The patient's skull was trepanned and the dura opened to allow visualization of the brain. The stereotactic tower was aligned to target and then the rigid cannulas were inserted into the brain along the planned track trajectory. The patient was awoken and Microelectrode recording (MER) was then carried out to physiologically identify the target nucleus with the intent of correcting any targeting inaccuracy. An O-arm image was then obtained with the cannula and microelectrode at the target. Additional parallel tracks were made if necessary. Once the ideal track was determined, the microelectrode was then withdrawn, and the DBS lead inserted.

The same procedure is then repeated on the contralateral side. O-arm CT images are taken after insertion of the microcannula on the second side, and then again after final placement of both DBS leads. Following closure, the fiducials are removed and the patient is then taken for a second post-operative fine-cut CT scan.

2.2. Computational Methods

We use a physics-based real-time adaptive deformable registration method [6] customized to register 3D pre-operative and intra-operative images for DBS (Figure 1). Given pre-operative MRI and CT, and intra-operative MR (iMR) or CT (iCT), we aim to find a deformation field between them and then deform the pre-operative MRI according to this field. The main idea of the physics-based non-rigid registration method [5] is to use the known displacement vector associated with sparse feature points in the brain to estimate the entire brain deformation using a regularization term based on a brain biomechanical model [3]. This method includes four critical components: (i) Segmentation and Mesh Generation; generate a patient-specific model, (ii) Feature point detection; identify small image blocks that have rich structural information in the pre-operative MRI, and (iii) Block matching; calculate displacement for each image block to generate a sparse deformation field, and the main computational step the (iv) Finite Element Solver which is used to estimate entire brain deformation based on the sparse deformation field computed at the block matching step (Figure 1). The pre-processing steps i.e., the segmentation, mesh generation of the brain images, feature point selection and block matching are described in [6, 7].

However, in this paper instead of using a tetrahedral mesh we use a hexaderal mesh which is more robust for CT images with higher noise than MRI. Given the noise in CT scans and the fact that the relevance of a displacement estimated with a block matching algorithm depends on the existence of highly discriminative structures within a block, we briefly focus on the feature selection and block matching. We use the variance of the image intensity within the block region to measure its relevance and only select a fraction of all potential blocks based on a predefined parameter of the algorithm. To avoid redundancy by the overlapping of blocks (i.e., eliminate blocks which are too close to each other), a parameter of prohibited connectivity is used. There are three options for the connectivity: vertex, edge and face connectivity (Figure 2). In addition to various connectivity patterns are supported in the ITK implementation, in this paper we use the face connectivity since it allows us to leverage the high confidence landmarks from the lead. Block matching is a well-known technique widely used in motion coding, image processing and compression. It is based on the assumption that a complex non-rigid transformation can be approximated by point-wise translations of small image regions. Considering an image block in a floating image and a predefined search window in a reference image, the block matching algorithm searches for a position in the reference image that maximizes a similarity measure M. Similarity measures in this task include mean square difference of intensity (MSD), mutual information (MI), and normalized cross correlation (NCC) [2]. By assembling the individual displacement vectors, one can create a sparse displacement field D, which the finite element solver will use to approximate the unknown displacement vector associated with the mesh vertices.

2.2.1. Parallel Finite Element Solver

The Parallel Finite Element Solver (PFEMS) estimates the mesh deformations from an approximation to an interpolation-based formulation while it rejecting the feature

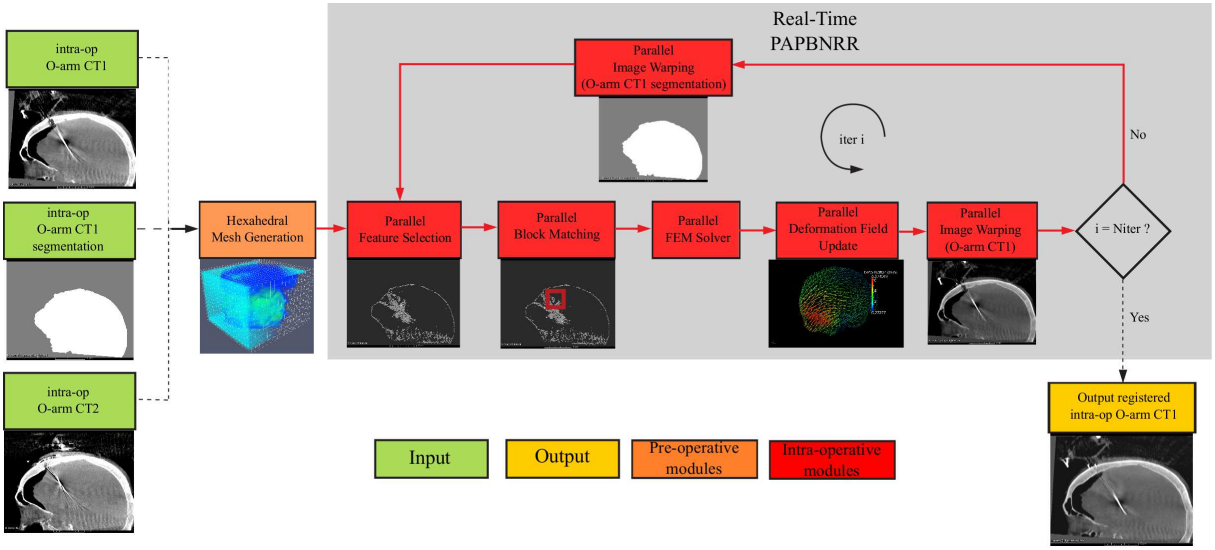

Figure 1. Software architecture of the Parallel Adaptive Physics-Based Non-Rigid Registration method (PAPBNR). The red boxes indicate that the computation is utilizing multiple cores and the gray boxes the existing ITK modules. The red arrows show the execution order of the different modules. The loop breaks when the desired number of iterations N_{iter} has reached.

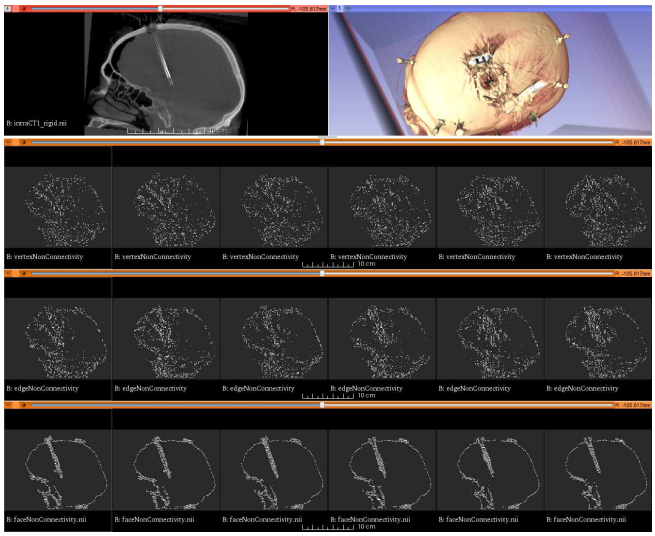

Figure 2. The distribution of the selected blocks in a brain CT scan, using different connectivity patterns. The results are depicted on six consecutive slices. From top to bottom row: sagittal CT slice (left) and volumetric rendering (right), selected blocks with "vertex" connectivity, selected blocks with "edge" connectivity, selected blocks with "face" connectivity. The "vertex" pattern results in a more uniform distribution, while the "face" pattern results in a higher block density nearby the lead and the tissue boundaries.

outliers (blocks with a large error between the computed mesh deformations and the block matching displacements). Figure 3 depicts PFEMS. K_b, K_m are the $N \times N$ stiffness matrices of the blocks and the mesh, respectively. $K_g = K_b + K_m$ is the $N \times N$ stiffness matrix of the biomechanical model. F is the block displacement vector of size N, with $N = 3 \cdot N_n$ and N_n is the number of the mesh vertices. The parallel outlier rejection loop depicted in Figure 3, for each iteration j, it removes $(N_b \cdot F_r)/N_{appr}$ blocks with the largest error between the computed mesh deformations and the block matching displacements. N_b is the number of selected image blocks, N_{appr} is the number of outlier rejection steps, and F_r controls the fraction of the rejected blocks. The PFEMS and all its parameters are described in detail at [6].

2.2.2. Analysis

The patient specific biomechanical non-rigid registration algorithm described above estimates the deformation that occurs between any two images. In particular, the registration algorithm accurately tracks highly radiopaque structures, such as the flexible electrode lead. Our hypothesis is that the deformation in the flexible electrode approximates the deformation in the deformable soft tissue (which is radiolucent). The deformations produced between successive intra-operative images is first visualized, and qualitatively evaluated. We describe the deformation in the region of interest near to the deep basal ganglia nuclei, or in a diameter of 1cm around the flexible electrode lead. Next, the recovered deformation fields are then used to deform the pre-operative scan. Using this newly updated image, we measure the locations of the relevant nuclei and characterize the brain shift that accounts for this movement.

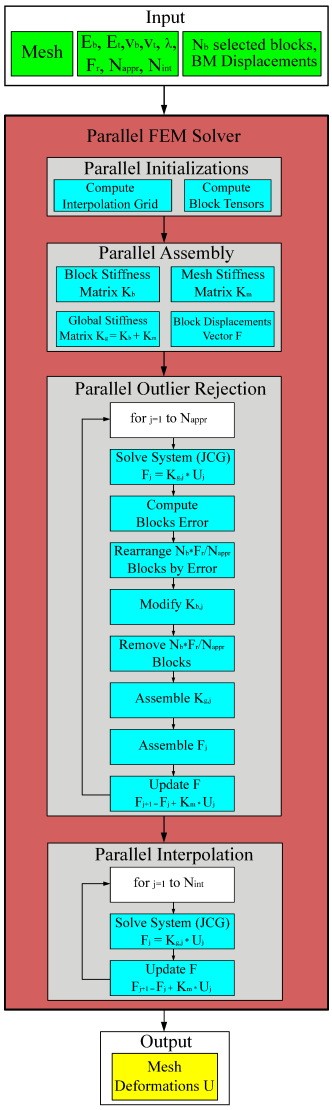

Figure 3. The Parallel FEM Solver (PFEMS) [6]. Green represents the input, gray represents the main steps (i.e., initializations, assembly, outlier rejection, and interpolation), cyan represents the components of each step, and yellow represents the output (i.e., mesh deformations U).

3. RESULTS

For each patient, we performed a deformable registration between O-arm CT1, and O-arm CT2 images. Table 1 lists the parameters of the registration. We identified the pre-operative and intra-operative positions of the relevant nuclei, and the deformation at the tip of the flexible lead from the deformed registered O-arm CT1. For the initialization of the non-rigid registration we performed a rigid alignment using Slicer's 4.4.0 BRAINSFit module [10]. Table 2 presents some quantitative results of the deformable registration. In all cases, the deformation is for the first side lead. In cases 1-2, the tip of the lead shifted primarily posteriorly and toward the side of the lead. In case 3, the lead shifted anteriorly and toward the side of the lead. In our future work we will include additional quantitative data regarding the shift in clinically important nuclei like the STN and the GPi in the MRIs, as well as additional measures of registration accuracy like the Hausdorff Distance. Figure 4 presents the qualitative evaluation results for case 1. The image discrepancies after our non-rigid registration are smaller compared to the rigid registration, particularly near the flexible electrode lead. Figure 5 depicts in more detail the recovered deformations for case 2. Figure 6 depicts qualitative evaluation results for case 3.

Table 1. The input parameters for the deformable registration (x: axial; y: coronal; z: sagittal).

Parameter	Units	Value	Description
Element type	-	8-node Hex	-
Similarity metric	-	NCC	Normalized Cross Correlation
F_s	-	5%	% selected image blocks
Connectivity pattern	-	"face"	-
$B_{s,x} \times B_{s,y} \times B_{s,z}$	voxels	$3 \times 3 \times 3$	Block size
$W_{s,x} \times W_{s,y} \times W_{s,z}$	voxels	$9 \times 9 \times 9$	Window size
$H_{s,x} \times H_{s,y} \times H_{s,z}$	-	$18 \times 18 \times 13$	Num Hexahedrons
E_b	Pa	2.1×10^3	Brain's Young modulus
ν_b	-	0.45	Brain's Poisson ratio
F_r	-	25%	% of rejected block outliers
N_{appr}	-	5	Num of outlier rejection steps
N_{int}	-	5	Num of interpolation steps
N_{iter}	-	1	Num of adaptive iterations

Table 2. Deformation (mm) at the tip of the flexible lead, end-to-end non-rigid registration time (including I/O) (seconds), and speed-up for the three clinical cases. The experiments conducted in a Linux workstation with 8 Intel i7-2600 @3.400 GHz CPU cores, and 16GB of RAM.

Case	Deformation (mm)		Time (sec)		Speed-Up
	Lead tip	Lead max	1 thread	8 threads	(T_1/T_8)
1	1.05	2.21	233.07	100.70	2.31
2	1.26	2.08	212.76	90.10	2.36
3	1.57	3.18	219.99	94.01	2.34

4. CONCLUSIONS

In this study we measured the brain shift that occurs during deep brain stimulation surgery by using flexible DBS leads as a radiopaque landmark in a biomechanical deformable registration method. We show how it is possible to recover the deformations that affect two clinically important nuclei of the basal ganglia. This technique can be applied intra-operatively to improve the targeting of DBS leads, and post-operatively to understand the nature of shift during DBS surgery. Future work includes characterizing how the brain shift occurs over time using multiple intra-operative images acquired during a single surgery. In addition, using pre- and post-operative

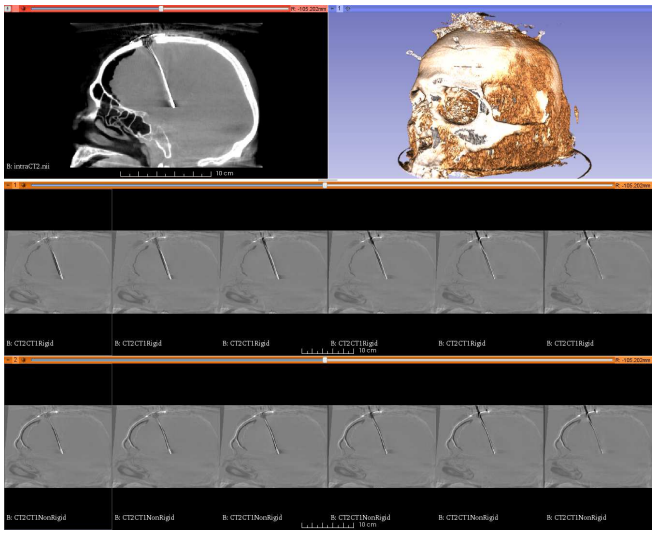

Figure 4. Qualitative results for case 1. Top row: intra-op O-arm CT2 (left) and its volume rendering (right). Middle row: Rigid registered O-arm CT1 subtracted from CT2. Bottom row: Deformable registered O-arm CT1 subtracted from CT2.

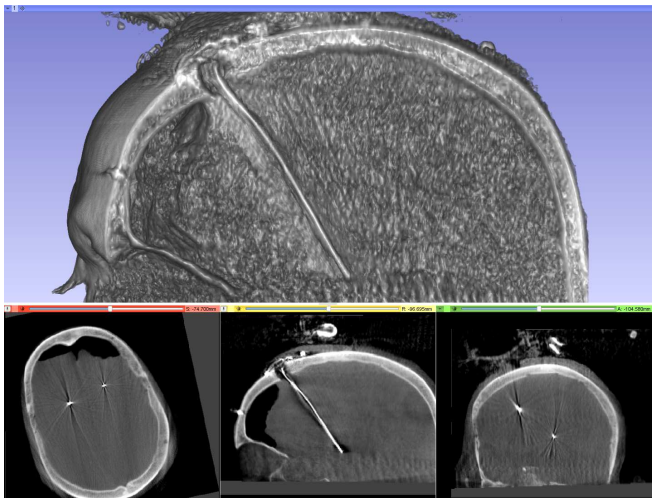

Figure 5. Deformable registered O-arm CT1 for patient 2. The shift is larger nearby the cortical structures and smaller in deep brain structures (tip of the lead). Top: cut section of a volume rendering. Bottom: axial, sagittal, and coronal slices.

MRI, it becomes possible to recover the entire time course of shift, including any that occurs before the first intra-operative image is captured. A better understanding of this shift, and the intra-operative correction of the same can, with future enhancements of this method, improve targeting accuracy and patient outcomes in DBS surgery.

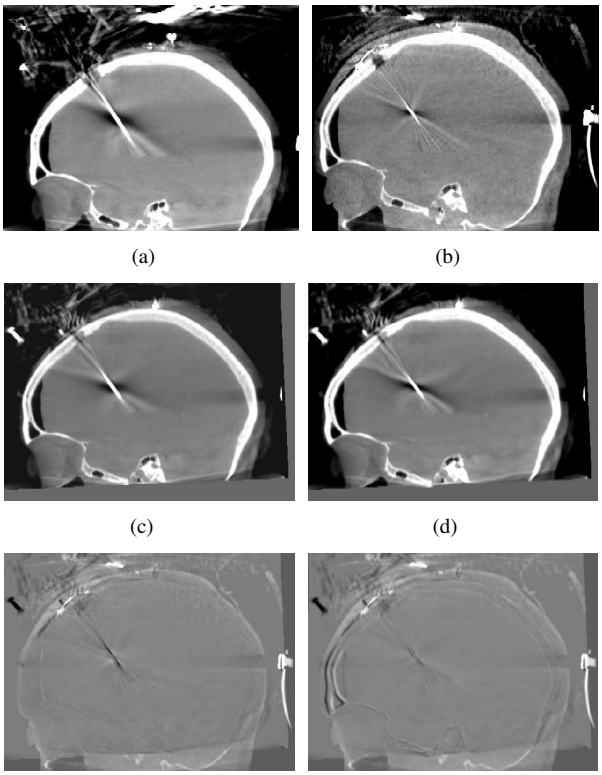

Figure 6. Qualitative evaluation results for case 3. (a)-(f) depict the same sagittal slice of the volumetric CT scan. (a): O-arm CT1; (b): O-arm CT2; (c): rigid registered O-arm CT1; (d): non-rigid registered O-arm CT1; (e): rigid registered O-arm CT1 subtracted from O-arm CT2; (f): non-rigid registered O-arm CT1 subtracted from O-arm CT2.

ACKNOWLEDGEMENTS

Research reported in this publication was supported in part by the Modeling and Simulation Fellowship at Old Dominion University, the Office of The Director, National Institutes Of Health under Award Number R44OD018334 the NSF grants: CCF-1139864 and CCF-1439079 and by the Richard T.Cheng Endowment. The content is solely the responsibility of the authors and does not necessarily represent the official views of the NIH and NSF.

REFERENCES

[1] P. Blomstedt and I. M. Hariz. Hardware-related complications of deep brain stimulation: a ten year experience. *Acta Neurochirurgica*, 147(10):1061–1064, 2005.

[2] L. G. Brown. A survey of image registration techniques. *ACM Comput. Surv.*, 24(4):325–376, Dec. 1992.

[3] O. Clatz, H. Delingette, I. F. Talos, A. J. Golby, R. Kikinis, F. A. Jolesz, N. Ayache, and S. K. Warfield. Robust

nonrigid registration to capture brain shift from intraoperative mri. *IEEE Transactions on Medical Imaging*, 24(11):1417–1427, Nov 2005.

[4] K. Doshi P. Long-term surgical and hardware-related complications of deep brain stimulation. *Stereotact Funct Neurosurg*, 89(2):89–95, 2011.

[5] F. Drakopoulos and N. P. Chrisochoides. *Computational Modeling of Objects Presented in Images. Fundamentals, Methods, and Applications: 4th International Conference, CompIMAGE 2014, Pittsburgh, PA, USA, September 3-5, 2014*, chapter A Parallel Adaptive Physics-Based Non-rigid Registration Framework for Brain Tumor Resection, pages 57–68. Springer International Publishing, Cham, 2014.

[6] F. Drakopoulos and N. P. Chrisochoides. Accurate and fast deformable medical image registration for brain tumor resection using image-guided neurosurgery. *Computer Methods in Biomechanics and Biomedical Engineering: Imaging & Visualization*, 4(2):112–126, 2016.

[7] F. Drakopoulos, Y. Liu, P. Foteinos, and N. P. Chrisochoides. Towards a real time multi-tissue adaptive physics based non-rigid registration framework for brain tumor resection. *Frontiers in Neuroinformatics*, 8(11), 2014.

[8] C. Hamani and A. M. Lozano. Hardware-related complications of deep brain stimulation: A review of the published literature. *Stereotact Funct Neurosurg*, 84(5-6):248–251, 2006.

[9] X. Hu, X. Jiang, X. Zhou, J. Liang, L. Wang, Y. Cao, J. Liu, A. Jin, and P. Yang. Avoidance and management of surgical and hardware-related complications of deep brain stimulation. *Stereotact Funct Neurosurg*, 88(5):296–303, 2010.

[10] H. Johnson, G. Harris, and K. Williams. Brainsfit: Mutual information registrations of whole-brain 3d images, using the insight toolkit, 10 2007.

[11] M. F. Khan, K. Mewes, R. E. Gross, and O. Skrinjar. Assessment of brain shift related to deep brain stimulation surgery. *Stereotact Funct Neurosurg*, 86:44–53, 2008.

[12] P. Van den Munckhof, M. F. Contarino, L. J. Bour, J. D. Speelman, R. M. A. de Bie, and P. R. Schuurman. The first evaluation of brain shift during functional neurosurgery by deformation field analysis. *Neurosurgery*, 67:49–54, 2010.

[13] D. Winkler, M. Tittgemeyer, J. Schwarz, C. Preul, K. Strecker, and J. Meixensberger. The first evaluation of brain shift during functional neurosurgery by deformation field analysis. *Journal of Neurology, Neurosurgery, and Psychiatry*, 76(8):1161–1163, 2005.